Supplementary Information

Restructuring of Ag catalysts for methanol to formaldehyde conversion studied using in situ X-ray ptychography and electron microscopy

Srashtasrita Das[1], Maik Kahnt[2], Youri van Valen[3], Tina Bergh[3], Sara Blomberg[4,5], Mikhail Lyubomirskiy[6], Christian G. Schroer[6], Hilde J. Venvik[3,*], Thomas L. Sheppard[1,‡,*]

[1]Institute for Chemical Technology and Polymer Chemistry, Karlsruhe Institute of Technology, 76131 Karlsruhe, Germany
[2]MAX IV Laboratory, Lund University, 22100 Lund, Sweden
[3]Department of Chemical Engineering, Norwegian University of Science and Technology, NO-7491 Trondheim, Norway
[4]NanoLund, Lund University, Box 118, 211 00 Lund, Sweden
[5]Department of Chemical Engineering, Lund University, Box 118, 221 00 Lund, Sweden
[6]Center for X-ray and Nano Science, Deutsches Elektronen-Synchrotron, 22607 Hamburg, Germany
‡Current address: Institute of Chemical Technology, Leipzig University, Linnéstrasse 3, 04103 Leipzig, Germany
Corresponding author(s), E-mail(s): thomas.sheppard@kit.edu, hilde.j.venvik@ntnu.no

Table of Contents

1. Nanoreactor setup

The Climate nanoreactor (DENSSolutions B.V., Delft, Netherlands) facilitates *in situ* transmission electron microscopy (TEM) studies by providing an enclosed gas-controlled environment. The nanoreactor setup consists of a MEMS-based TEM chip with a spiral-shaped micro heater and X-ray transparent silicon nitride (SiNx) windows for mounting samples. The MEMS-based Climate chips (compatible with JEOL scanning transmission electron microscope) can heat samples to 1000 °C. The chips are commercially available and offer precise temperature control. A second Si chip with a square-shaped SiNx membrane ensures an enclosed gas environment while being electron and X-ray transparent. The two chips are separated by an O-ring for gas-tight operation. The temperature of the mounted sample is monitored and controlled with a heating control unit and Digiheater software (DENSSolutions B.V., Delft, Netherlands).

To adapt the nanoreactor for synchrotron measurements, a beamline interface was developed in cooperation with the Sample Environment team at DESY. This allowed to accommodate the electrical contact needles and gas tubing. The implemented nanoreactor-beamline interface design is shown in **Supplementary Figure 1**. The gas supply to the nanoreactor was ensured by an in-house gas dosing system consisting of mass flow controllers (Bronkhorst High-Tech B.V., Ruurlo, Netherlands). The total gas flow rate was set to 0.5 ml/min. The gas feed input was connected to the nanoreactor from the right, and the outflow from the left side of the nanoreactor was connected to the beamline exhaust.

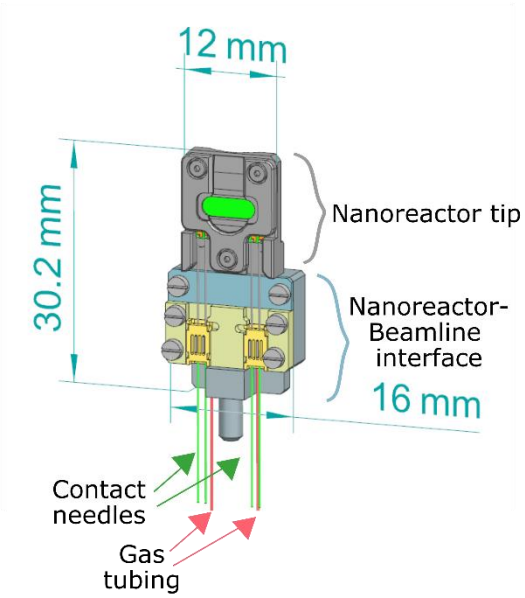

Figure S1: CAD design of the in-house developed nanoreactor-beamline interface implemented for its usage at the P06 beamline of PETRA III. This adaptation of the nanoreactor facilitates controlled temperature and gas environment for correlative *in situ* electron and X-ray microscopy.

2. Sample preparation and nanoreactor assembly

Samples were mounted on the MEMS-based TEM chips using the focused ion beam (FIB) milling and lift out (details described in the manuscript). The Ga+ beam induced deposition of Pt was utilized for positioning the samples on the MEMS-based chips. The mounting of the chips into the nanoreactor cell involved a separate assembly of the nanoreactor tip, followed by the integration of the nanoreactor-beamline interface. A link to the "Dos and Don'ts for Sample Preparation" document and a User Manual describing in detail all the required assembly steps are accessible within the DESY intranet (Confluence/XWiki Pages of FS-PETRA or FS-P06) for the assembly and usage of nanoreactor at the P06 beamline. These files are accessible for users with beamtime proposals accepted at P06.

3. *In situ* X-ray imaging

3.1. Synchrotron experiments

In situ 2D X-ray ptychography of Ag catalysts up to 650 °C was performed at the P06 beamline of PETRA III at the Deutsches-Elektronen Synchrotron DESY (Hamburg, Germany). The nanoreactor was integrated into the PtyNAMI setup of the nanoprobe endstation.[1] 2D ptychographic projections of the samples were obtained using a coherent X-ray beam with incident energy of 10.3 keV focused using nano-focusing lenses. The sample was scanned at an out-of-focus position, with a resultant beam size of ~0.4 µm (FWHM) and ~1 µm (FWHM) in the horizontal and vertical direction, respectively, on the sample plane. The resulting diffraction patterns were recorded using an EIGER X 4M (Dectris, Switzerland), a single photon counting detector with pixel size of 75 µm x 75 µm. Depending on the spot size and sample size, as shown in **Table S1**, the scan parameters were optimized for each sample to yield a data acquisition time of 4-5 mins per ptychographic projection.

Table S1: Experimental parameters for 2D X-ray ptychography at P06 beamline.

Scan step size (x-direction)	0.44-0.5 µm
Scan step size (y-direction)	0.44-0.63 µm
Beam size in the sample plane (FWHM; h)	0.4 µm (PHe), 0.4 µm (Air, PA1), 0.34 µm (Air, PA2)
Beam size in the sample plane (FWHM; v)	0.9 µm (Air, PA1), 0.8 µm (Air, PA2), 1.3 µm (PHe)
Exposure time per scan point	1.0 s (Air, PA1), 0.4 s (Air, PA2), 0.1 s (PHe)
Scan time per ptychographic projection	4-5 min
Photon energy	10.3 keV
Photon flux	4×10^7 photons/s
Sample-to-detector distance	3.2 m
Detector pixel size	75 µm x 75 µm

In situ X-ray ptychography of Ag catalysts up to 500 °C was performed at the NanoMAX beamline of the MAX IV Laboratory (Lund University, Lund, Sweden).[2] The nanoreactor was mounted at the diffraction endstation.[3] Kirkpatrick-Baez mirrors were used to focus the X-ray beam to a symmetric diffraction-limited focal spot of 100 nm (FWHM) at 10 keV incident photon energy. The reactor was placed 1.5 mm downstream of the X-ray beam focus position to increase the illuminated area of the sample to effectively 1.5 µm spot size, allowing for larger steps in the ptychographic scan. Resulting diffraction patterns were recorded using EIGER2 X 4M (Dectris, Switzerland) with a pixel size of 75 µm x 75 µm,[4] at a distance of 3.512 m from the source. All scans performed during the temperature cycles were acquired with the same parameters as shown in **Table S2**.

Table S2: Experimental parameters for 2D X-ray ptychography at NanoMAX beamline.

Scan step size (x- and y-direction)	0.4 µm (± 20% jitter)
Beam size in the sample plane (FWHM; h, v)	1.5 µm
Exposure time per scan point	0.1 s
Scan time per ptychographic projection	7 min 10 s
Scan area (h x v)	10.8 µm x 9.6 µm
Photon energy	10 keV
Photon flux	2 x 10^9 photons/s
Sample-to-detector distance	3.512 m
Detector pixel size	75 µm x 75 µm

3.2. X-ray ptychography data processing

For ptychographic reconstructions, each diffraction pattern obtained using EIGER X 4M was cropped to 512 x 512 pixels. 2000 iterations of the ePIE-based algorithm were implemented using the in-house *Ptycho* code of the P06 beamline. The projections were aligned using the translation transformation via an iterative pyramidal approach available in the StackReg plugin of Fiji (an ImageJ distribution) on the phase unwrapped ptychographic projections.[5] Final corrections to the registration of this projection series were carried out manually. The uncovered region of the SiNx membrane of the Climate chip was used for the removal of phase ramps and global phase offsets, and hence background correction. The ptychographic reconstructions obtained at the P06 had an effective pixel size of 10.0 nm.

The ptychographic projections obtained at the NanoMAX beamline were reconstructed using diffraction patterns cropped to 256 x 256 pixels. The PtyPy framework[6] was used to reconstruct each projection using 100 iterations of the difference-map (DM) algorithm,[7] followed by 1900 iterations of the maximum-likelihood (ML) algorithm.[8] Relative image alignment was performed after the removal of arbitrary phase offsets and gradients using persistent prominent edges in the recorded projections and using the "phase_cross_correlation" function from the "scikit-image" module for Python.[9] The ptychographic reconstructions had an effective pixel size of 22.7 nm.

4. Image-based assessment for stability and dynamic study

4.1. Determination of structural stability as a function of temperature under different gas environments

P06 beamline, DESY: The observed changes in ptychographic projection series used for the study of bubble growth and expansion, followed by subsequent movement of material for all measured samples are shown in **Figure S2-S7**.

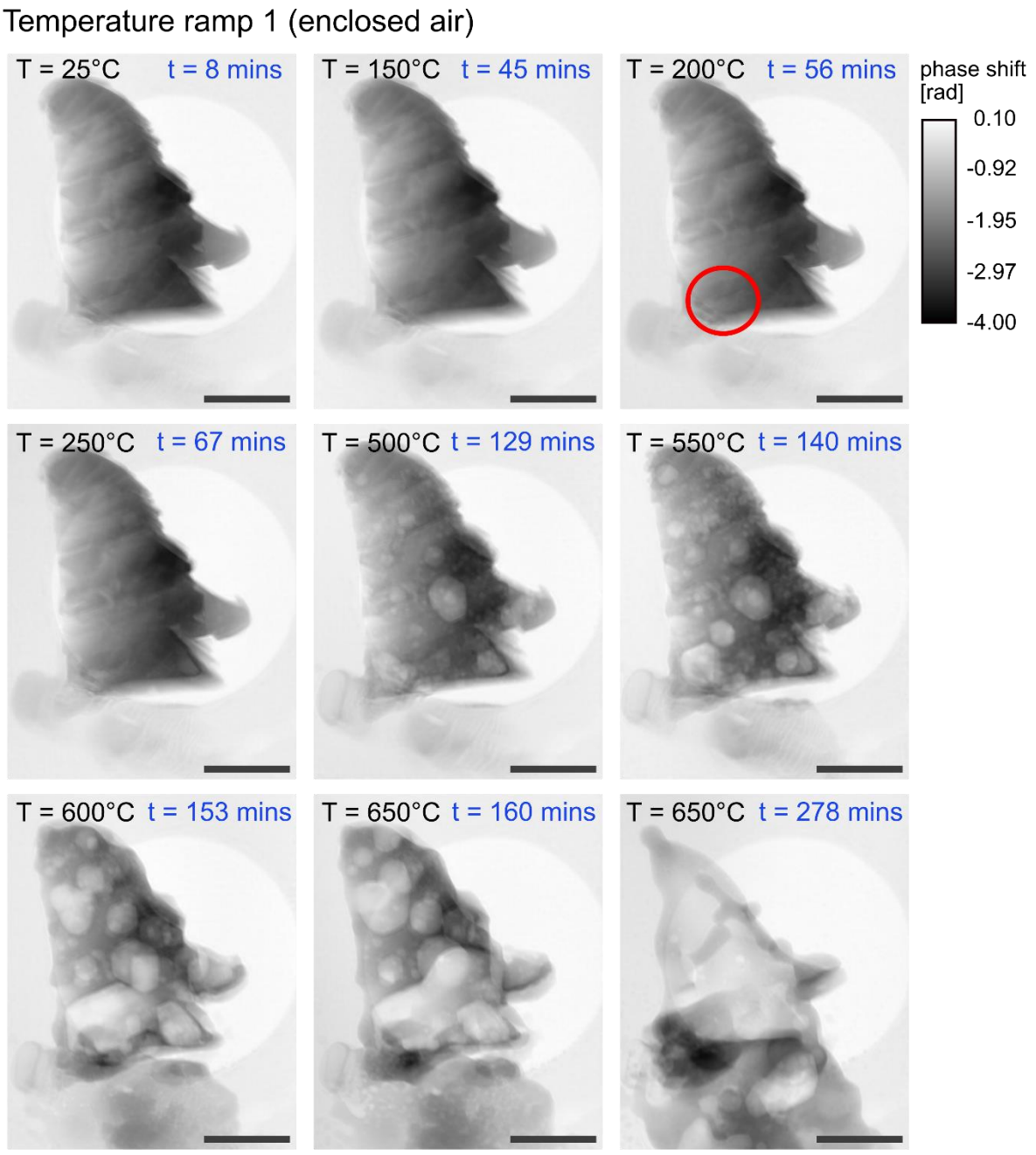

Figure S2: The bubble growth visualization and catalyst restructuring study upon exposure to air (sample PA1) as a function of reaction temperature. The red circle highlights the initial bubble formation. All scale bars: 2.4 µm.

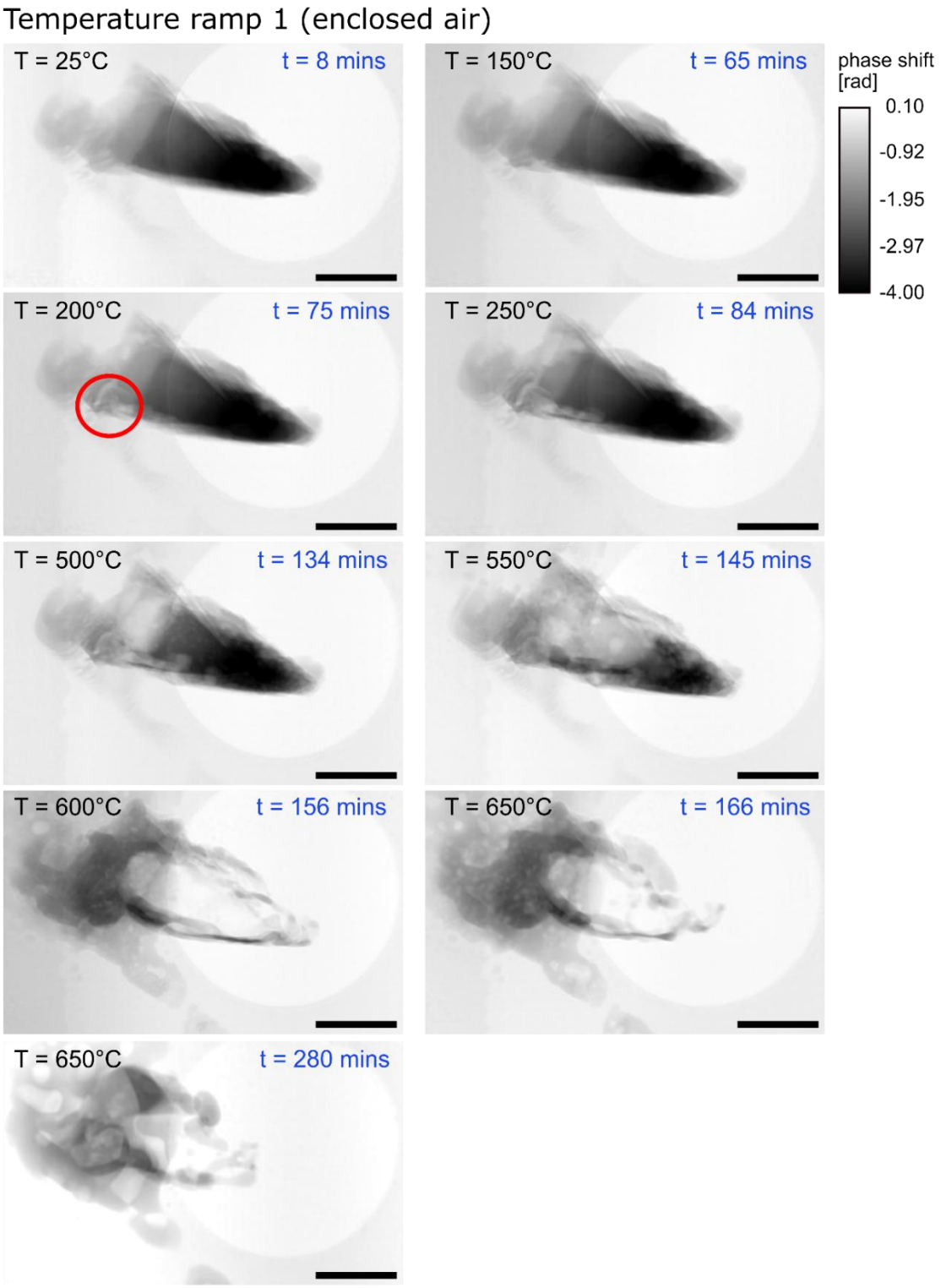

Figure S3: The bubble growth visualization and catalyst restructuring study upon exposure to air (sample PA2) as a function of reaction temperature. The red circle highlights the initial bubble formation. All scale bars: 2.4 µm.

The above samples were further exposed to a second temperature ramp up to 650 °C, followed by a stable temperature maintained at 650 °C for around 2 hours under ambient air. Respective details are shown in **Figure S4-S5**.

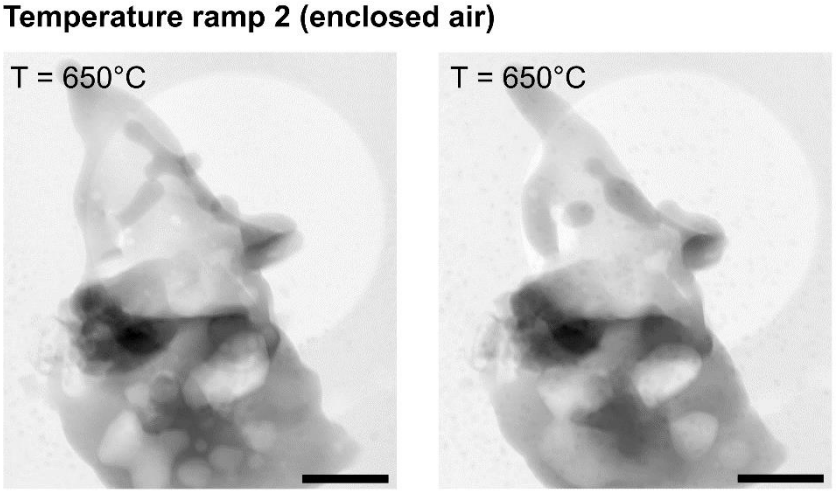

Figure S4: The sample PA1 before and after the second temperature ramp, exhibiting comparatively less significant changes. All scale bars: 2 µm.

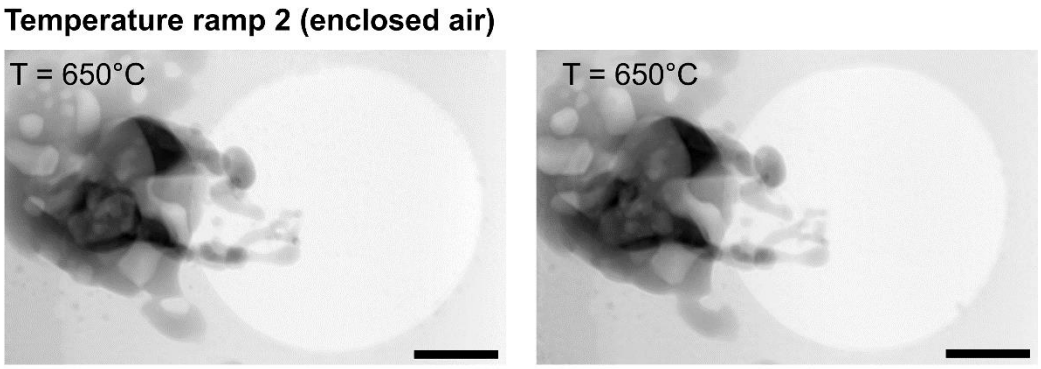

Figure S5: The sample PA2 before and after the second temperature ramp, showing no or negligible changes. All scale bars: 2 µm.

Since these samples showed less or no significant changes in the net movement of material, they were not analyzed further for an extended study of the influence of the reaction environment during the second temperature ramp.

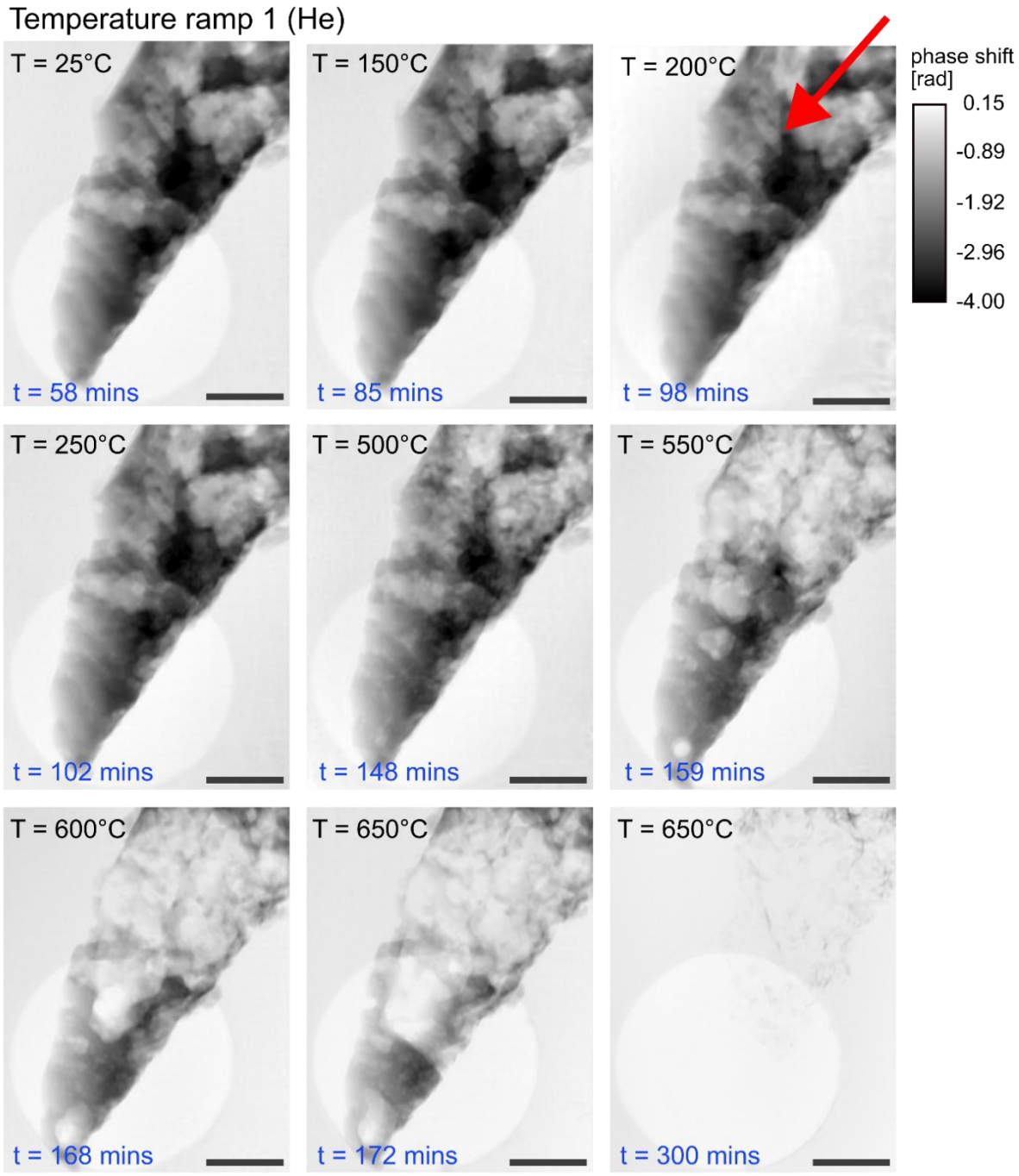

Figure S6: The bubble growth visualization and catalyst restructuring study upon exposure to He (sample PHe) as a function of reaction temperature. The red arrow shows the formation and direction of bubble propagation. All scale bars: 2.4 µm.

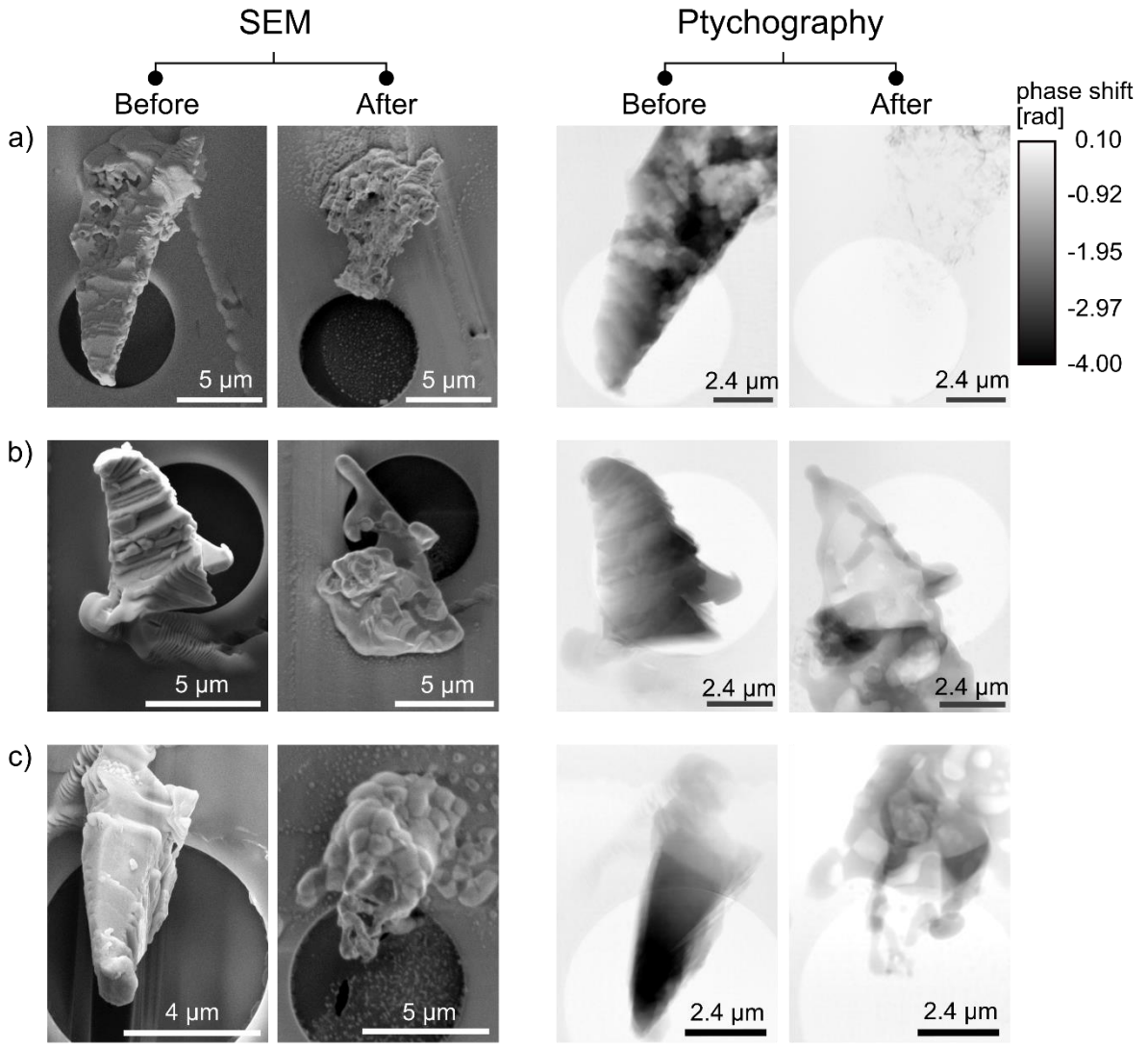

Figure S7: SEM and X-ray ptychography images of the samples a) PHe, b) PA1, and c) PA2, obtained before and after the exposure to their respective reaction environments.

After the first constant-temperature condition at 650 °C, the sample PHe was momentarily accidentally heated up to 1000 °C during the sample cooling. This explains the higher material restructuring observed for the sample PHe in the post-mortem SEM image of Fig. S7a, compared to PA1 and PA2.

NanoMAX beamline, MAX IV Laboratory: The samples measured for the dynamic study of catalyst during bubble formation and growth changes, when heated up to 500 °C under different gas environments, are shown in **Figure S8-S11**.

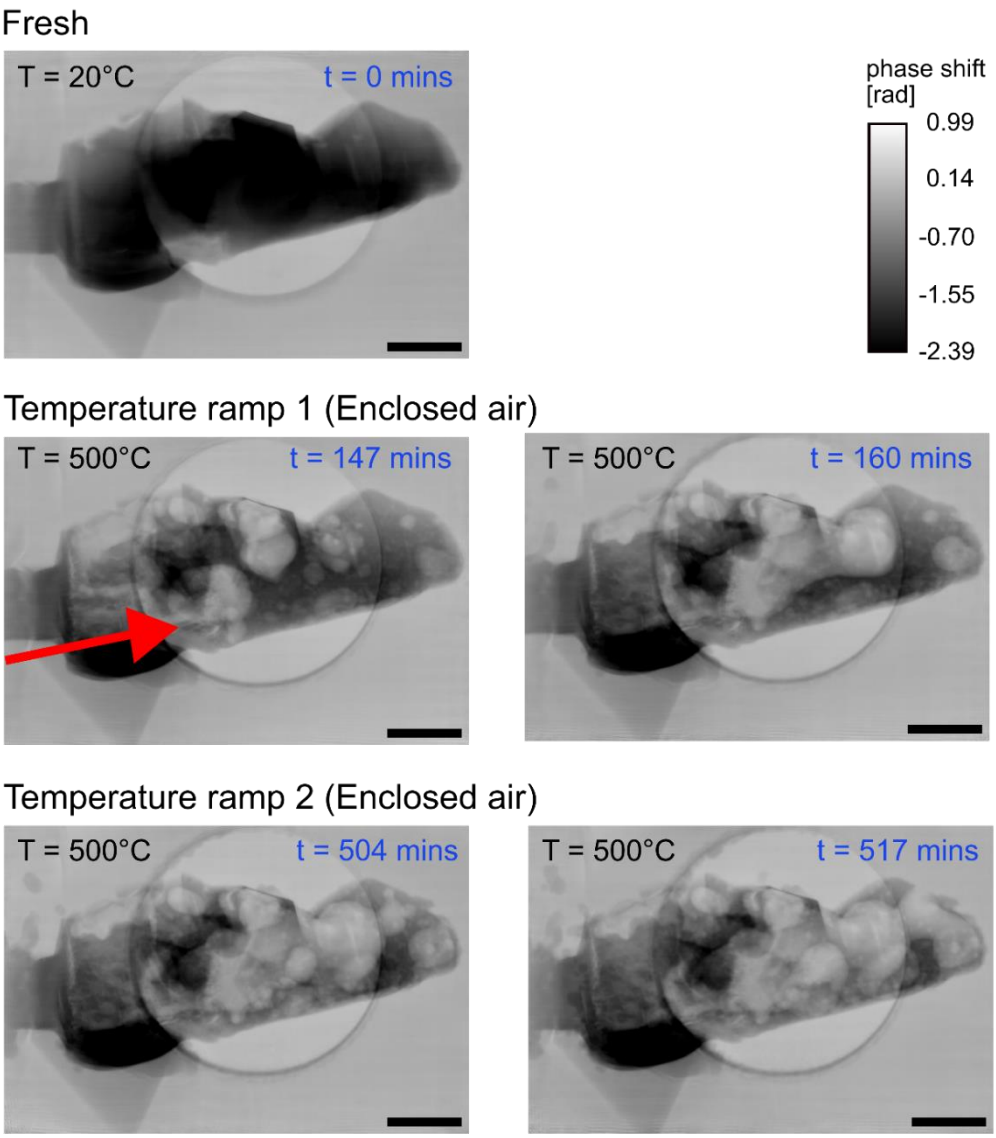

Figure S8: The bubble growth dynamics and catalyst restructuring study of sample MA1 for fresh catalyst (top row). Visualized before (left column) and after (right column) exposure to enclosed air at 500 °C, during the first temperature ramp (middle row) and the second temperature ramp (bottom row), upon exposure to ambient air. The red arrow shows the formation and direction of bubble propagation. All scale bars: 2 µm.

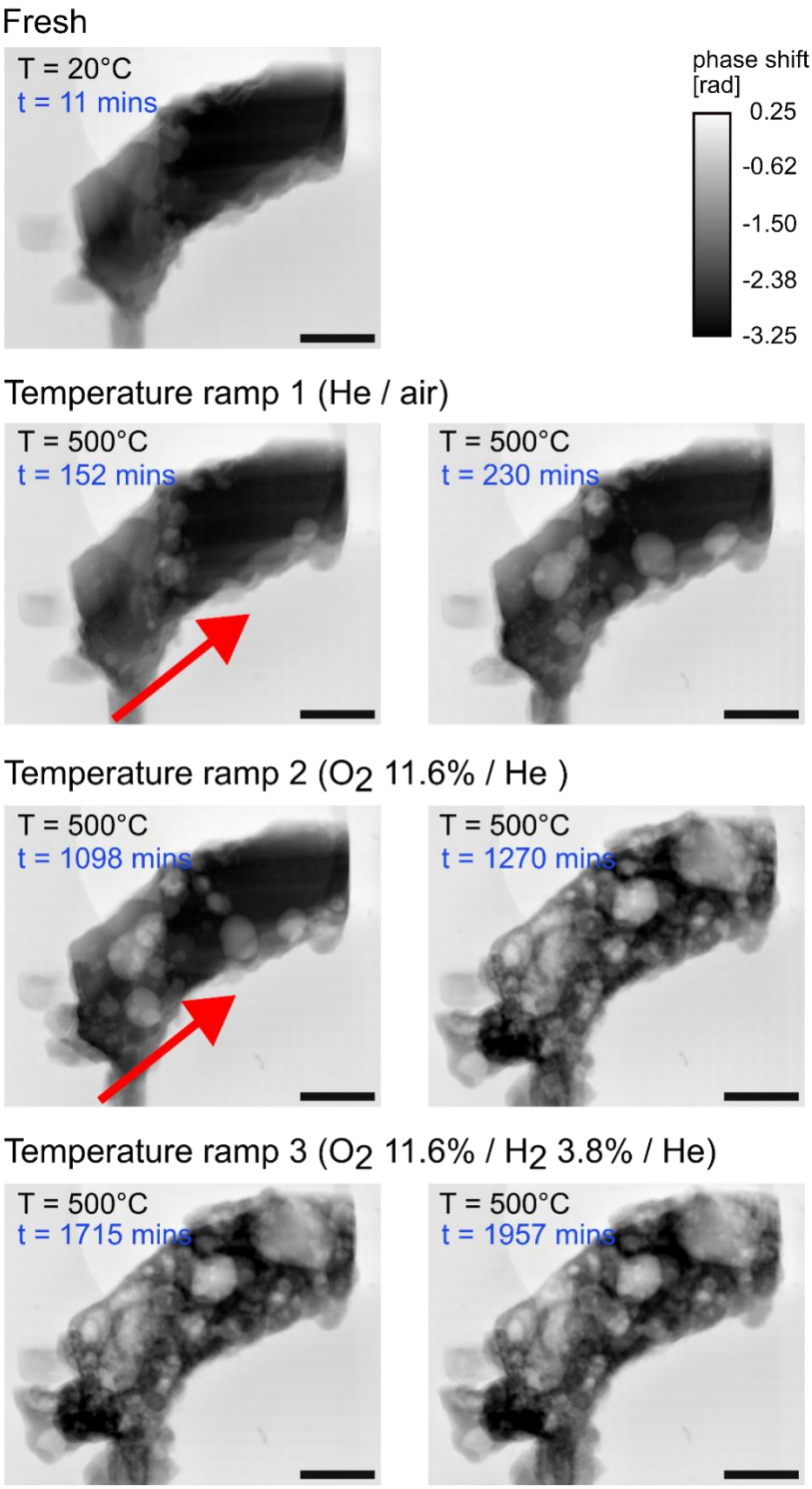

Figure S9: The bubble growth dynamics and catalyst restructuring study of sample MA2 for fresh catalyst (top row), followed by before (left column) and after (right column) exposure to various gas environments at 500 °C in the following order – exposure to He / air at (Temperature ramp 1), O_2 11.6% / He (Temperature ramp 2), O_2 11.6% / H_2 3.8% / He (Temperature ramp 3). The red arrows show the formation and direction of bubble propagation. All scale bars: 2 µm.

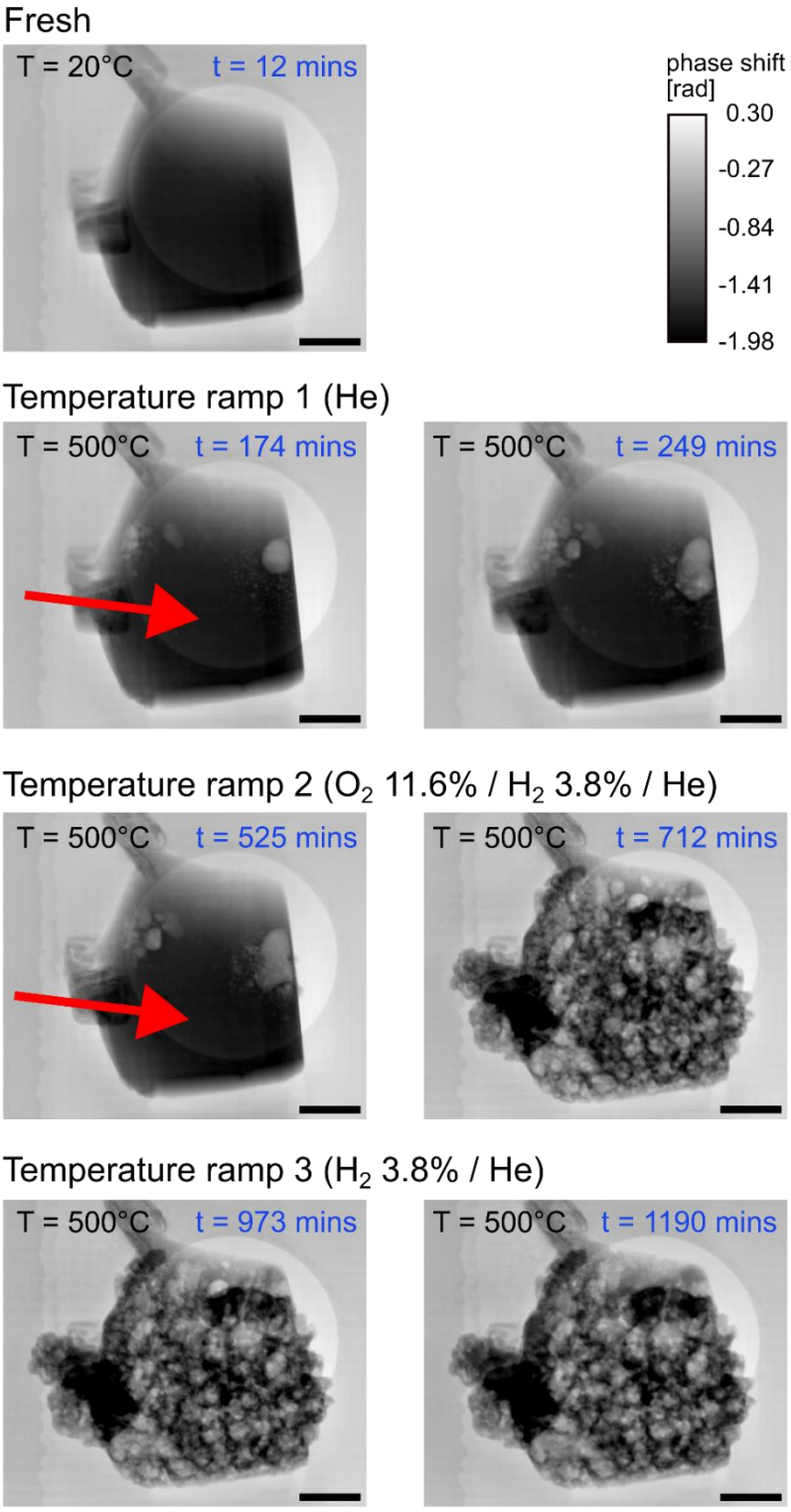

Figure S10: The bubble growth dynamics and catalyst restructuring study of sample MHe for fresh catalyst (top row), followed by before (left column) and after (right column) exposure to various gas environments at 500 °C in the following order – He (Temperature ramp 1), O_2 11.6% / H_2 3.8% / He at 500 °C (Temperature ramp 2), H_2 3.8% / He at 500 °C (Temperature ramp 3). The red arrow shows the formation and direction of bubble propagation. All scale bars: 2 µm.

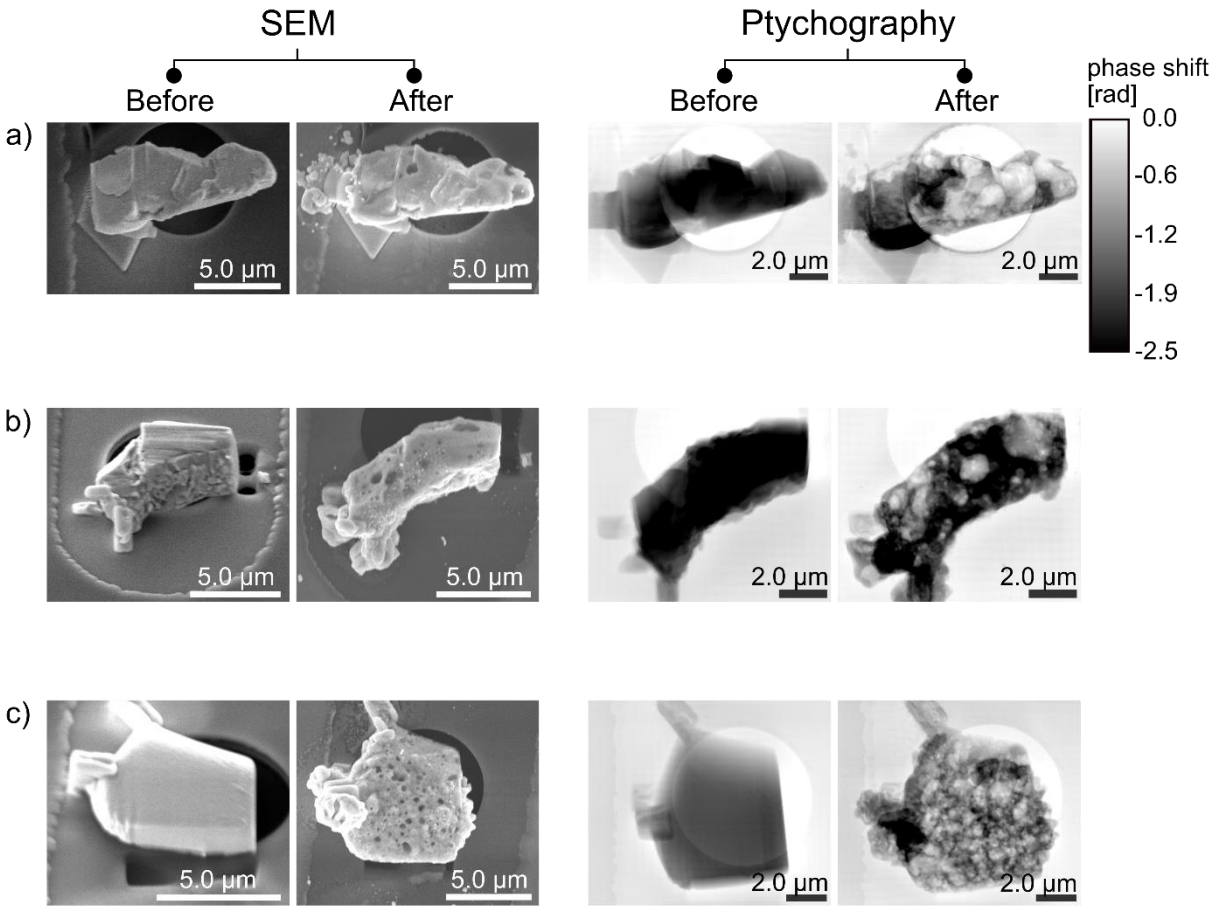

Figure S11: The SEM and X-ray ptychography images of the samples a) MA1, b) MA2, and c) MHe obtained before and after the exposure to their respective reaction environments.

4.2. Determination of bubble formation and propagation

The projections were masked, with the X-ray transparent SiNx membrane of the circular window chosen as the region of interest to ensure uniformity in the sample background. This region of interest was used to study dynamic changes in the catalyst. The selected region of interest for 3 samples tested at P06 beamline and NanoMAX beamline are shown in **Figure S12** and **Figure S13**, respectively.

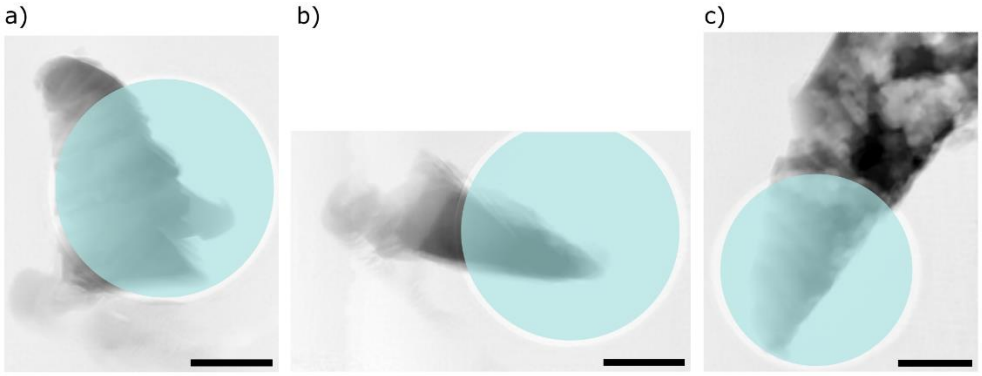

Figure S12: The selected region of interest illustrated on the three fresh samples measured at DESY: a) PA1, b) PA2, and c) PHe. All scale bars: 2.4 µm.

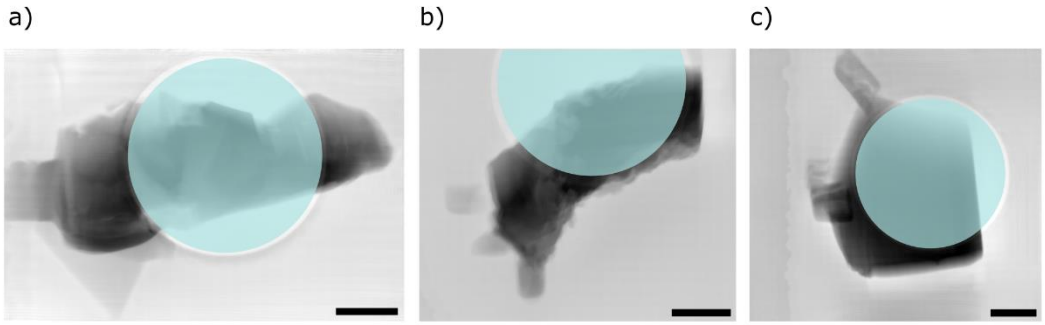

Figure S13: The selected region of interest illustrated on the three fresh samples measured at NanoMAX: a) MA1, b) MA2, and c) MHe. All scale bars: 2 µm.

The resultant integrated phase shift in the selected regions was plotted for all samples to demonstrate changes in relative mass and the associated rates of change, as shown in **Figures S14-15**.

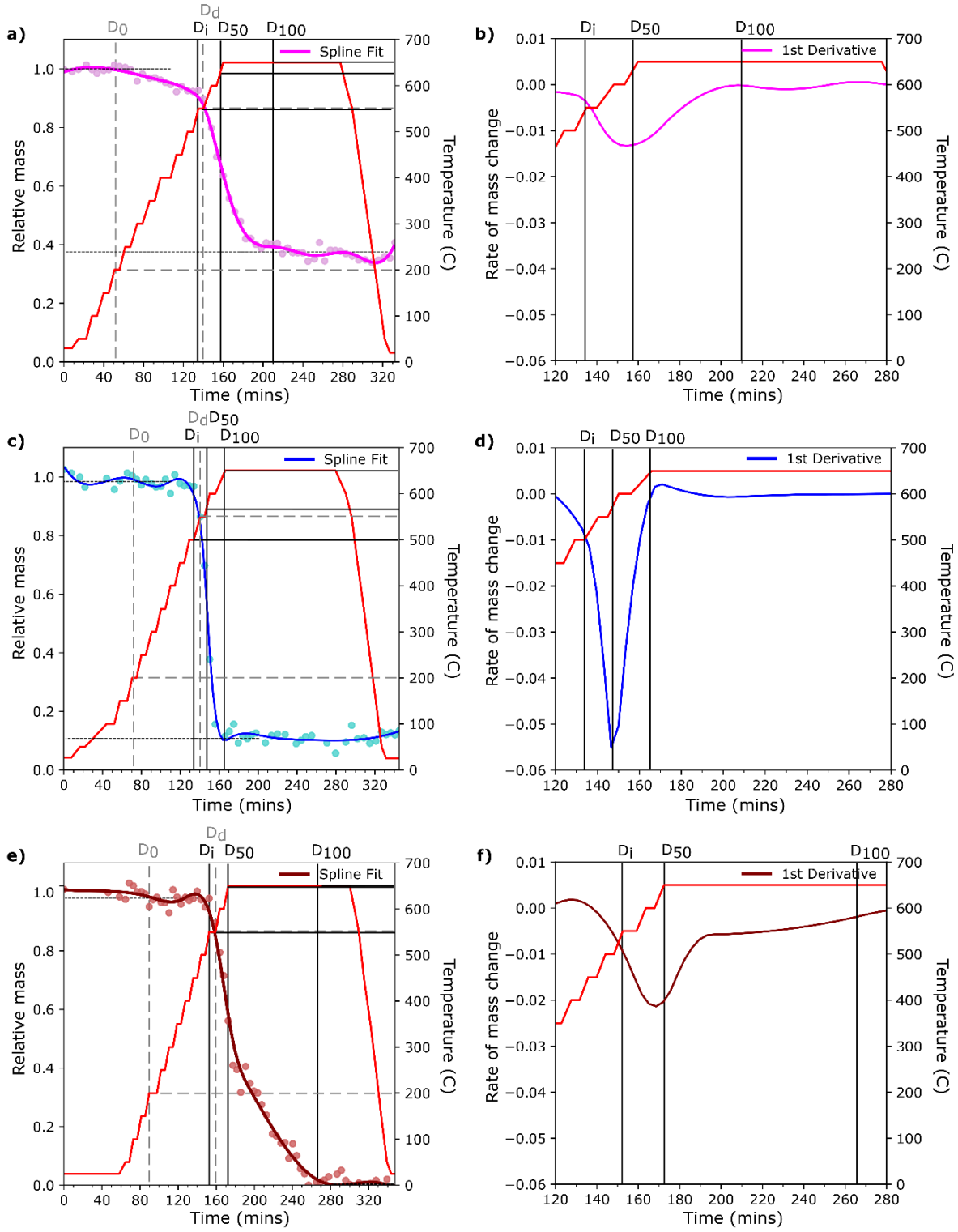

Figure S14: The changes in relative mass (left column) and their respective rate of change of mass (right column) for the samples aged under different gas conditions, a-b) PA1, c-d) PA2, and e-f) PHe, within the regions of interest shown in **Figure S12**.

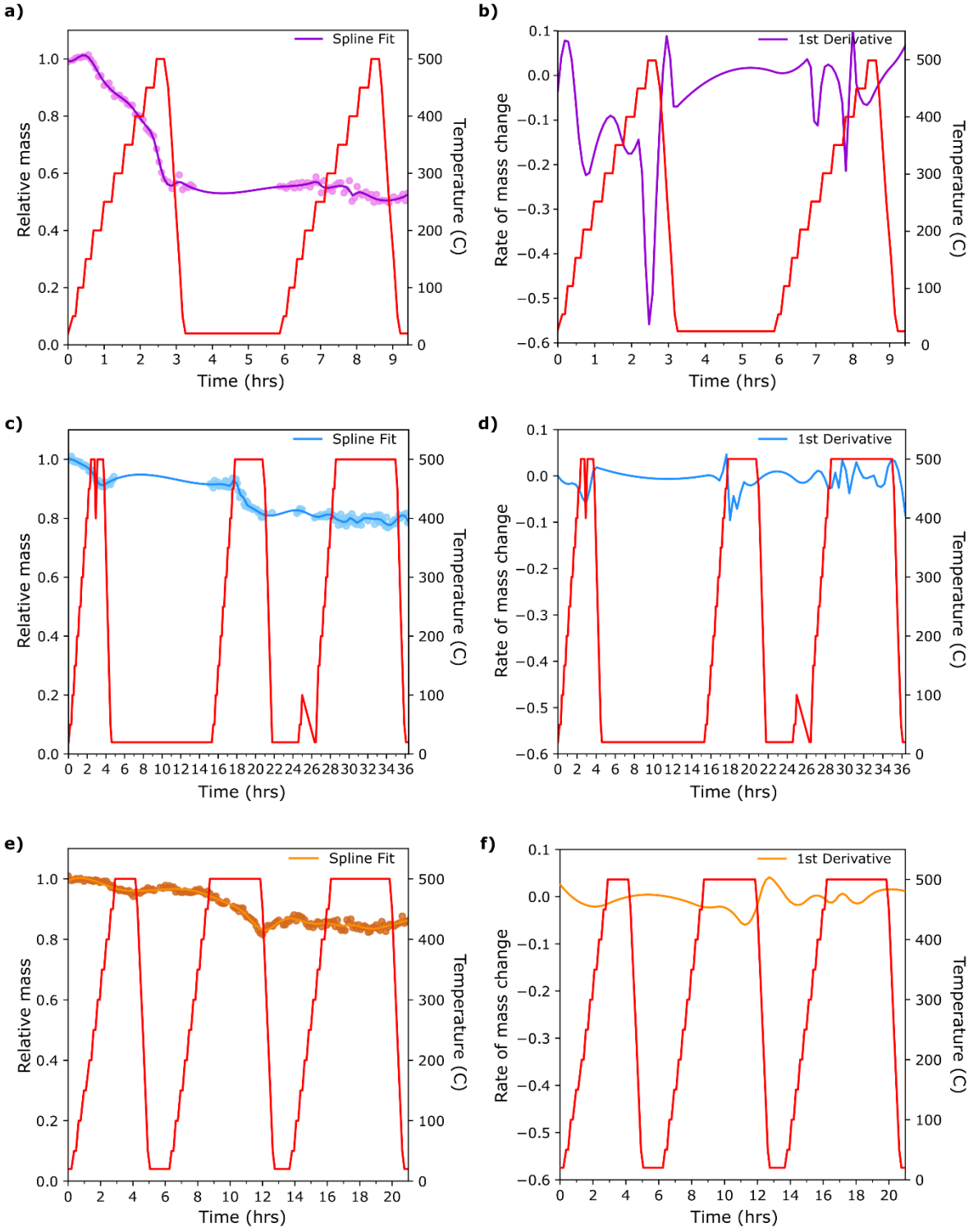

Figure S15: The changes in relative mass (left column) and their respective rate of change of mass (right column) for the samples aged under different gas conditions, a-b) MA1, c-d) MA2, and e-f) MHe, within the regions of interest shown in **Figure S13**.

The quantitative assessment of the samples treated up to 500 °C is been summarized in **Tables S3-S4** and **Figure S16**.

Table S3: Summary of estimated quantitative metrics for the fitted plot (shown in Figure 5, main text).

	Sample MA1				Sample MA2				Sample MHe			
	r-value	R^2	P-value	Std. dev	r-value	R^2	P-value	Std. dev	r-value	R^2	P-value	Std. dev
TR 1	-0.99	0.98	0.00	0.04	-0.90	0.81	0.00	0.02	-0.83	0.69	0.00	0.01
TR 2	-0.39	0.15	0.61	0.01	-0.94	0.88	0.00	0.04	-0.96	0.92	0.00	0.04
TR 3	-	-	-	-	-0.22	0.05	0.13	0.01	-0.31	0.10	0.09	0.01

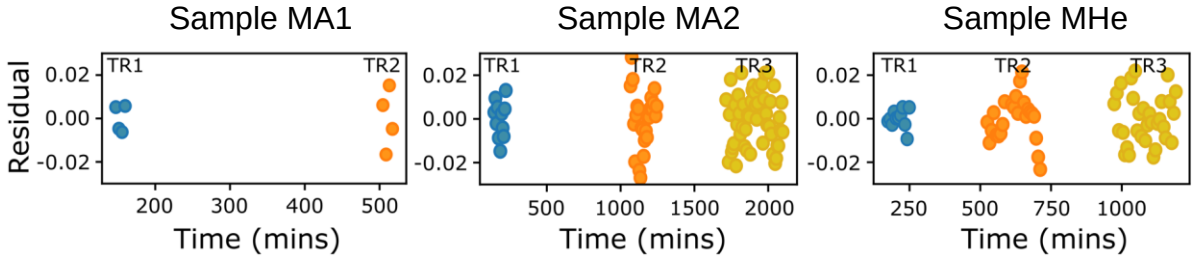

Figure S16: The distribution of calculated residuals for the fitted plot (shown in Figure 5, main text) as a function of time for each temperature ramp has been plotted for all 3 samples.

Table S4: Maximum and minimum relative mass values at the start and end of each temperature ramp (TR).

	Sample MA1			Sample MA2			Sample MHe		
	Y_max	Y_min	Δ	Y_max	Y_min	Δ	Y_max	Y_min	Δ
TR 1	0.680	0.574	0.106	0.958	0.907	0.051	0.968	0.950	0.018
TR 2	0.520	0.507	0.013	0.910	0.798	0.112	0.953	0.844	0.109
TR 3	-	-		0.796	0.787	0.009	0.849	0.837	0.012

5. Ex situ electron microscopy

The focused ion-beam milling using Ga for preparation of samples cut to desired length scales leads to Ga implantation and redeposition. In order to secure the prepared specimens on the MEMS-based TEM chips, the Methylcyclopentadienyl [Trimethyl] Platinum was used as a precursor to facilitate Ga+ beam induced deposition of Pt. This deposited material consequently contains Ga, C, and O in addition to Pt. This has been previously studied in literature.[10,11] As a result of this sample preparation procedure, the Ag catalyst also contains Pt and Ga in the region that was exposed to the ion beam and/or deposited Pt. To understand the possible influence of these materials, post-mortem SEM-EDX mapping was performed for samples treated at the P06 beamline (**Section 5.1)** and NanoMAX beamline (**Section 5.2)**.

5.1. Post-mortem chemical analysis for samples aged up to 650 °C

For samples aged up to 650 °C at the P06 beamline, the acquired elemental distribution maps of the samples mounted on the MEMS chips are shown in **Figure S17-S19**.

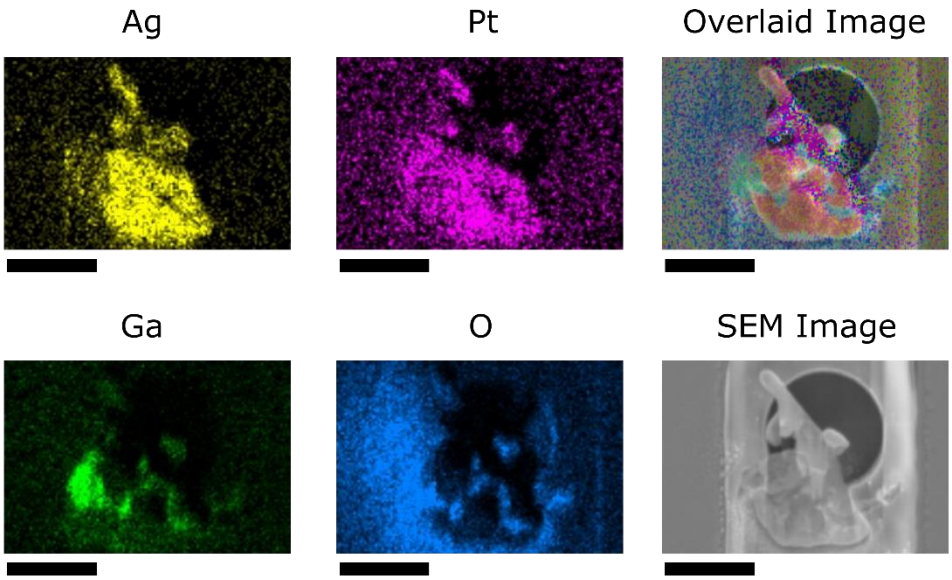

Figure S17: SEM-EDX maps of sample PA1 for the study of the distribution of silver (Ag), platinum (Pt), gallium (Ga), and oxygen (O), accompanied by an overlay of all elements (Overlaid Image). The SEM image shows a high-fidelity representation of the selected region of interest. All scale bars: 10 µm.

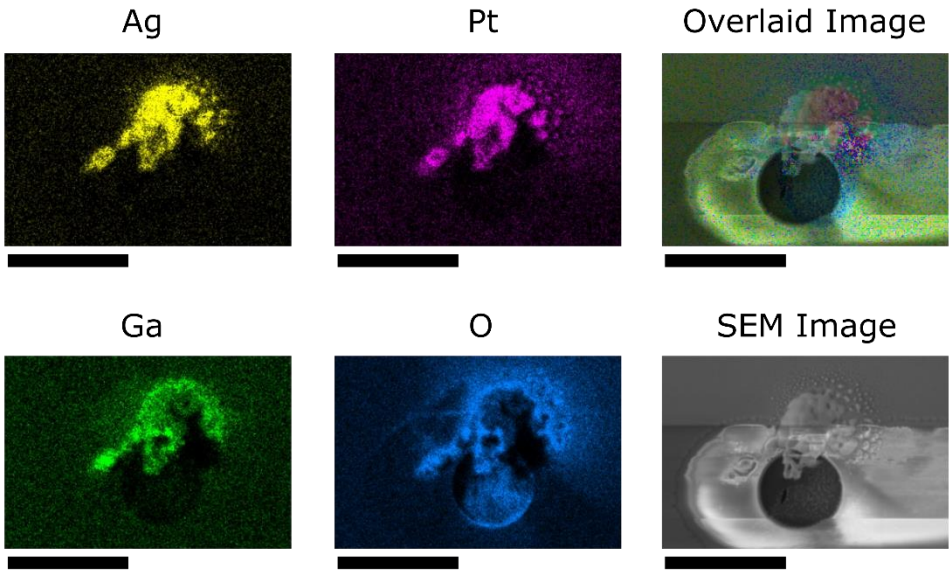

Figure S18: SEM-EDX maps of sample PA2 for the study of the distribution of silver (Ag), platinum (Pt), gallium (Ga), and oxygen (O), accompanied by an overlay of all elements (Overlaid Image). The SEM image shows a high-fidelity representation of the selected region of interest. All scale bars: 10 µm.

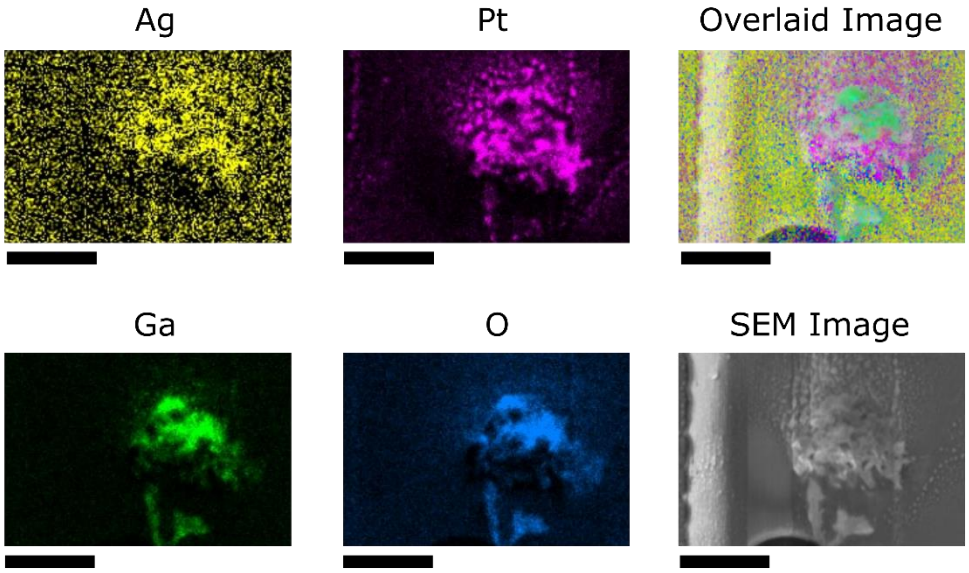

Figure S19: The SEM-EDX maps of PHe for the study of the distribution of silver (Ag), platinum (Pt), gallium (Ga), and oxygen (O), accompanied by an overlay of all elements (Overlaid Image). The SEM image shows a high-fidelity representation of the selected region of interest. All scale bars: 5 µm.

5.2. Post-mortem chemical analysis for samples aged up to 500 °C

For samples aged up to 500 °C at the NanoMAX beamline, the acquired elemental distribution maps of the samples mounted on the MEMS chips are shown in **Figure S20**.

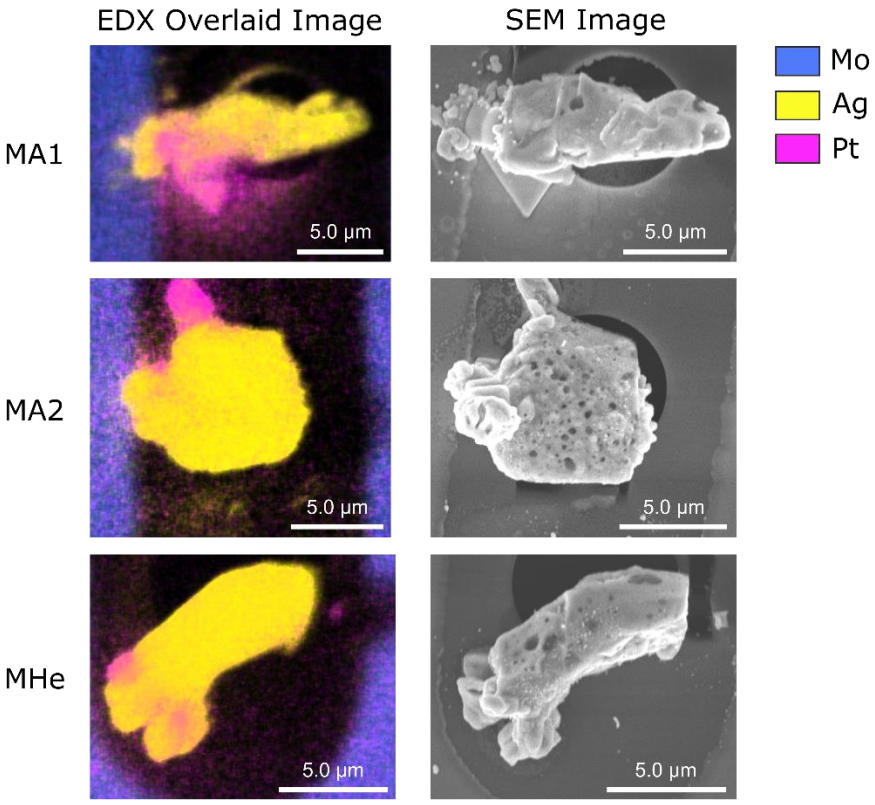

Figure S20: The SEM-EDX maps of samples MA1 (top row), MA2 (middle row), and MHe (bottom row) for the study of the distribution of silver (Ag) and platinum (Pt). Each sample shows an overlay of both elements (EDX Overlaid Image). The SEM image shows a high-fidelity representation of the selected region of interest.

References

1. Schroer, C. G. *et al.* PtyNAMi: ptychographic nano-analytical microscope at PETRA III: interferometrically tracking positions for 3D x-ray scanning microscopy using a ball-lens retroreflector. in *Proc.SPIE* vol. 10389 103890E (2017).

2. Johansson, U. *et al.* NanoMAX: the hard X-ray nanoprobe beamline at the MAX IV Laboratory. *J. Synchrotron Radiat.* **28**, 1935–1947 (2021).

3. Carbone, D. *et al.* Design and performance of a dedicated coherent X-ray scanning diffraction instrument at beamline NanoMAX of MAX IV. *J. Synchrotron Radiat.* **29**, 876–887 (2022).

4. Donath, T. *et al.* EIGER2 hybrid-photon-counting X-ray detectors for advanced synchrotron diffraction experiments. *J. Synchrotron Radiat.* **30**, 723–738 (2023).

5. Thevenaz, P., Ruttimann, U. E. & Unser, M. A pyramid approach to subpixel registration based on intensity. *IEEE Trans. Image Process.* **7**, 27–41 (1998).

6. Enders, B. & Thibault, P. A computational framework for ptychographic reconstructions. *Proc. R. Soc. A Math. Phys. Eng. Sci.* **472**, 20160640 (2016).

7. Thibault, P., Dierolf, M., Bunk, O., Menzel, A. & Pfeiffer, F. Probe retrieval in ptychographic coherent diffractive imaging. *Ultramicroscopy* **109**, 338–343 (2009).

8. Thibault, P. & Guizar-Sicairos, M. Maximum-likelihood refinement for coherent diffractive imaging. *New J. Phys.* **14**, 63004 (2012).

9. van der Walt, S. *et al.* scikit-image: image processing in Python. *PeerJ* **2**, e453 (2014).

10. Utke, I., Hoffmann, P. & Melngailis, J. Gas-assisted focused electron beam and ion beam processing and fabrication. *J. Vac. Sci. Technol. B Microelectron. Nanom. Struct. Process. Meas. Phenom.* **26**, 1197–1276 (2008).

11. Langford, R. M., Wang, T.-X. & Ozkaya, D. Reducing the resistivity of electron and ion beam assisted deposited Pt. *Microelectron. Eng.* **84**, 784–788 (2007).